EVS28
KINTEX, Korea, May 3-6, 2015

Dynamic Wireless Power Transfer System for Electric Vehicle to Simplify Ground Facilities - Power Control Based on Vehicle-side Information -

Katsuhiro Hata[1], Takehiro Imura[1], Yoichi Hori[1]
[1]*The University of Tokyo, 5-1-5, Kashiwanoha, Kashiwa, Chiba, Japan, hata@hflab.k.u-tokyo.ac.jp*

Abstract

Electric vehicles (EVs) have environmental advantages and the capacity for advanced motion control. However, EVs need to be charged frequently due to their limited mileage per charge. A dynamic wireless power transfer (WPT) system for EVs can extend their cruising distance and reduce the size of their energy storage system. However, when being applied to rugged roadways over long distances, it is important to simplify ground facilities as much as possible. While it is practical for a static system to control both side using communication, a dynamic system for EVs should be controlled only on the vehicle-side. To implement a suitable control system, this paper focuses on vehicle-side control for achieving a required power and proposes a control method based on road-side voltage estimation using only vehicle-side information. Conventional methods have proposed voltage control using a DC-DC converter on the vehicle-side while road-side voltage is regulated to obtain a reference value. However, this causes ground facilities to become complicated due to a need for a feedback system. The proposed method estimates road-side voltage, therefore eliminating the need for its regulation. As a result, ground facilities can be simplified. The estimation equation is based on the equivalent circuit of a WPT system and expressed as a function of vehicle-side voltage and current. The reference value and the equilibrium point of the DC-DC converter can be obtained by the estimated road-side voltage. Therefore, the power control system with a voltage controller can be designed. The estimation equation and the power control are verified by experiments. These results suggest that the proposed method can achieve the required power without controlling the road-side or communicating between a vehicle and ground facilities.

Keywords: Wireless power transfer, Magnetic resonant coupling, Dynamic charging system, Primary voltage estimation, Power control

1 Introduction

Electric vehicles (EVs) have not only environmental advantages but also the capacity for advanced motion control. Their electric motors have the advantages of a faster and more accurate toque response over internal combustion engines [1]. However, EVs need to be charged frequently due to their limited mileage per charge. It is important to make a charging network and to reduce the burden on the user.

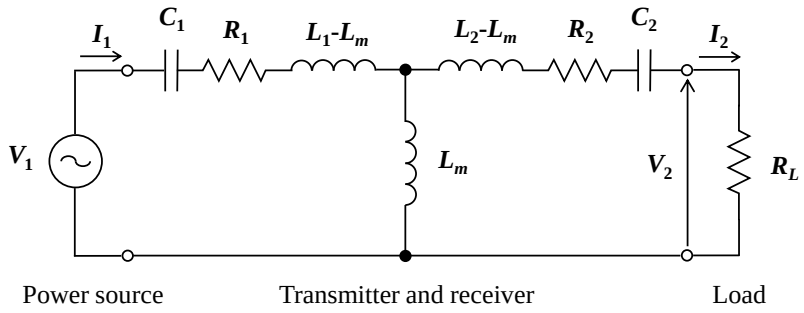

Figure 1: Equivalent circuit of wireless power transfer via magnetic resonant coupling.

Wireless power transfer (WPT) can mitigate complicated charging operations by eliminating the use of wiring. In recent years, a dynamic WPT system for moving EVs has gathered attention [2]-[8]. It can extend the cruising distance of EVs and reduce the size of the energy storage system of EVs. However, when being applied to rugged roadways over long distances, it is important to simplify ground facilities as much as possible. In addition, highly efficient transmission and a stable supply of power have to be achieved regardless of a change in position of the receiver, which is equipped in a vehicle.

WPT via magnetic resonant coupling can achieve a highly efficient mid-range transmission and it has robustness to misalignment of the transmitter and the receiver [9], [10]. The transmitting efficiency and charging power are determined not only by the parameters of the transmitter and the receiver but also by the load [11], [12]. The load condition can be controlled by using a DC-DC converter on the vehicle-side [13]-[16]. Previous research [17] has proposed voltage control on the vehicle-side for efficiency maximization. However, this control method has to regulate the road-side voltage and complicates ground facilities.

This paper proposes a control method based on road-side voltage estimation using only vehicle-side information. The proposed method can control the charging power regardless of the road-side voltage, therefore eliminating the need for its regulation. As a result, ground facilities can be simplified.

2 Wireless Power Transfer via Magnetic Resonant Coupling

2.1 Input/output characteristics at resonance frequency

This paper uses a series-series (SS) circuit topology of WPT via magnetic resonant coupling and its equivalent circuit is shown in Figure 1 [18]. The transmitter and the receiver are composed of the inductances L_1, L_2, the series-resonance capacitances C_1, C_2, and the internal resistances R_1, R_2. L_m is the mutual inductance between L_1 and L_2. V_1 and I_1 are the root-mean-square voltage and current on the primary-side, which is the road-side. V_2 and I_2 stand for the root-mean-square voltage and current on the secondary side, which is the vehicle-side. R_L is the load resistance. The transmitter and the receiver are designed to satisfy the equation, which is expressed as follows:

$$\omega_0 = \frac{1}{\sqrt{L_1 C_1}} = \frac{1}{\sqrt{L_2 C_2}} \tag{1}$$

where ω_0 is the power source angular frequency.

Then, the voltage ratio A_V and the current ratio A_I between the secondary-side and the primary-side are expressed as follows:

$$A_V = \frac{V_2}{V_1} = j\frac{\omega_0 L_m R_L}{R_1 R_2 + R_1 R_L + \left(\omega_0 L_m\right)^2} \tag{2}$$

$$A_I = \frac{I_2}{I_1} = j\frac{\omega_0 L_m}{R_2 + R_L}. \tag{3}$$

As a result, the transmitting efficiency η is described as follows:

$$\eta = \frac{\left(\omega_0 L_m\right)^2 R_L}{\left(R_2 + R_L\right)\left\{R_1 R_2 + R_1 R_L + \left(\omega_0 L_m\right)^2\right\}}. \tag{4}$$

Furthermore, the load power P is given as follows:

$$P = \frac{A_V^{\,2}}{R_L} V_1^2. \tag{5}$$

Table 1: Characteristics of transmitter and receiver.

	Primary side	Secondary side
Resistance R_1, R_2	1.15 Ω	1.20 Ω
Inductance L_1, L_2	636 μH	637 μH
Capacitance C_1, C_2	40000 pF	39940 pF
Resonant frequency f_1, f_2	99.8 kHz	99.8 kHz
Outer diameter	448 mm	
Number of turns	56 turns	

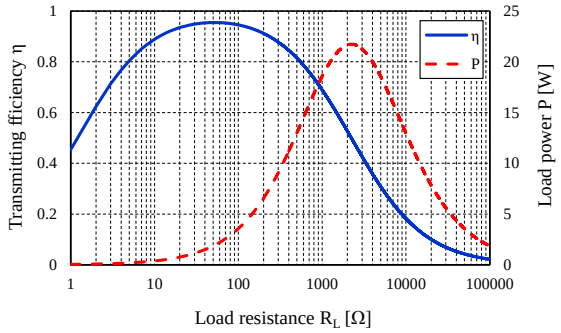

Figure 2: Transmitting efficiency and load power versus load resistance.

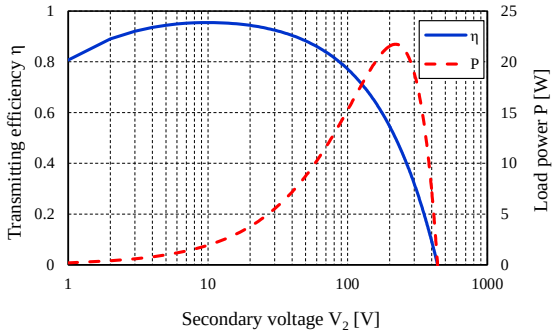

Figure 3: Transmitting efficiency and load power versus secondary voltage.

The transmitting efficiency and the load power are determined by the parameters of the coil, the resonance frequency, and the load resistance. Figure 2 shows the transmitting efficiency and the load power versus the load resistance. Then, the coil parameters are indicated in Table 1 and the mutual inductance L_m is 80.8 μH. The amplitude of V_1 is 10 V and its frequency is 99.8 kHz. When the transmitting efficiency is maximized, the load resistance $R_{L\eta\max}$ is expressed as follows:

$$R_{L\eta\max} = \sqrt{R_2\left\{\frac{\left(\omega_0 L_m\right)^2}{R_1} + R_2\right\}}. \qquad (6)$$

The maximum load power is obtained when the load resistance $R_{LP\max}$ is given as follows:

$$R_{LP\max} = \frac{\left(\omega_0 L_m\right)^2}{R_1} + R_2 . \qquad (7)$$

2.2 Voltage control on vehicle side

Figure 3 shows the transmitting efficiency and the load power versus the secondary voltage under the same conditions as Figure 2. From these figures, the equivalent load resistance is increased in response to the increase in the secondary voltage.

The secondary voltage $V_{2\eta\max}$, which maximizes the transmitting efficiency, is described as follows:

$$V_{2\eta\max} = \sqrt{\frac{R_2}{R_1}}\frac{\omega_0 L_m}{\sqrt{R_1 R_2 + \left(\omega_0 L_m\right)^2} + \sqrt{R_1 R_2}} V_1. \qquad (8)$$

In order to achieve maximum efficiency, a secondary voltage control system should be designed to satisfy eq. (8).
Power control can also be achieved by the secondary voltage control. However, it is effective only if the secondary voltage is controlled below the maximum secondary voltage $V_{2\max}$, which is expressed as follows:

$$V_{2\max} = \frac{\omega_0 L_m}{R_1} V_1. \qquad (9)$$

Then, the equivalent load resistance goes to infinity and the voltage ratio A_V becomes saturated [11]. The maximum power is obtained when the secondary voltage $V_{2P\max}$ is given as follows:

$$V_{2P\max} = \frac{\omega_0 L_m}{2R_1} V_1 = \frac{1}{2} V_{2\max}. \qquad (10)$$

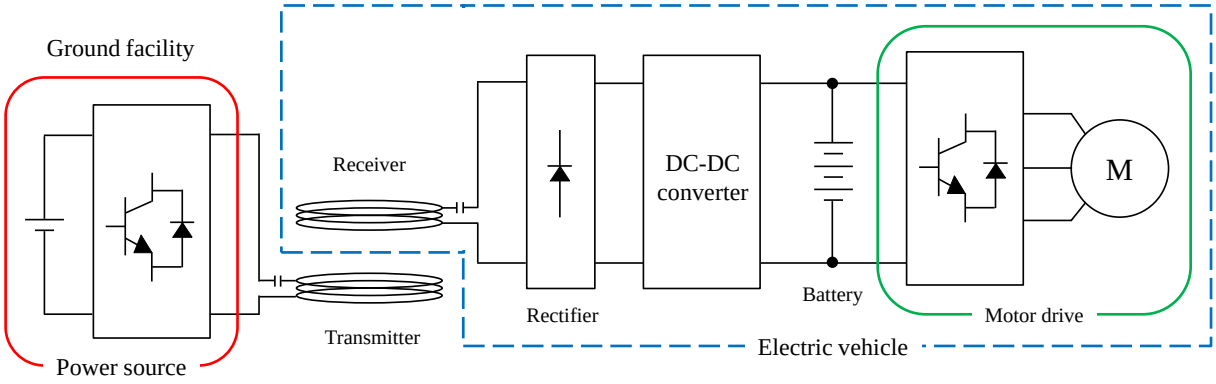

Figure 4: System configuration for power control on vehicle-side.

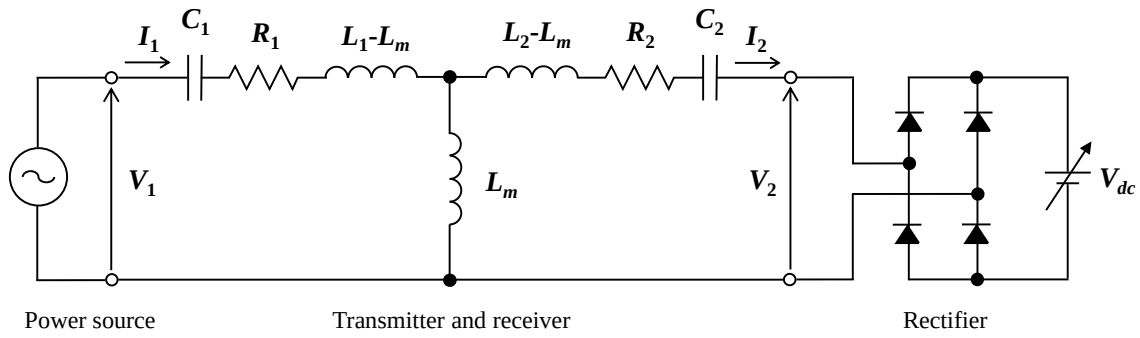

Figure 5: Circuit diagram of wireless power transfer system.

In order to achieve the required power P^*, the secondary voltage control system is designed. Figure 4 shows the system configuration for power control on the vehicle-side. The DC-DC converter can control the output voltage of the rectifier. As a result, the secondary voltage can be also controlled. For efficient transmission, it is important to define the operating range of the secondary voltage to be below $V_{2P\max}$. As a result, the reference value of the secondary voltage V_2^* can be expressed as follows:

$$V_2^* = V_{2P\max} - \sqrt{V_{2P\max}^2 - \frac{\left\{R_1 R_2 + (\omega_0 L_m)^2\right\} P^*}{R_1}}. \quad (11)$$

Then, $V_{2P\max}$, which is obtained by eq. (10), includes information of the primary voltage V_1. However, it is undesirable to require communication between a vehicle and ground facilities, and to regulate the primary voltage. Therefore, this paper proposes an estimation method of the primary voltage using only vehicle-side information.

3 Primary Voltage Estimation

3.1 Circuit analysis with phasors

Assuming that the secondary voltage control is designed properly, the circuit diagram of the WPT system can be indicated in Figure 5.

When the SS circuit topology is used, the secondary current can be assumed to be a sinusoidal wave oscillating at the resonant frequency with its phase advanced 90 degrees from the primary voltage [19]. If it is assumed that the diodes conduct according to the secondary current, the secondary voltage becomes a square wave, which has the same amplitude as the DC voltage V_{dc}, the same phase as the secondary current and the resonant frequency. Therefore, the phasor of the secondary voltage is given by a Fourier series expansion and expressed as follows:

$$\dot{V}_2 = j\frac{2\sqrt{2}}{\pi} V_{dc}. \quad (12)$$

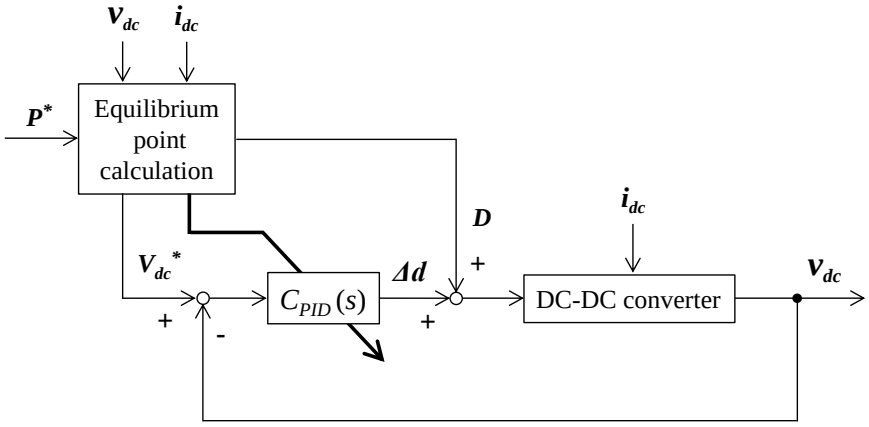

Figure 6: Block diagram of power control.

At the resonant frequency, the circuit equation can be expressed as follows:

$$\begin{bmatrix} \dot{V}_1 \\ \dot{V}_2 \end{bmatrix} = \begin{bmatrix} R_1 & j\omega_0 L_m \\ j\omega_0 L_m & R_2 \end{bmatrix} \begin{bmatrix} \dot{I}_1 \\ \dot{I}_2 \end{bmatrix}. \quad (13)$$

From eq. (12), eq. (13) is transformed as follows:

$$\begin{bmatrix} \dot{I}_1 \\ \dot{I}_2 \end{bmatrix} = \begin{bmatrix} R_1 & j\omega_0 L_m \\ j\omega_0 L_m & R_2 \end{bmatrix}^{-1} \begin{bmatrix} V_1 \\ j\frac{2\sqrt{2}}{\pi} V_{dc} \end{bmatrix}. \quad (14)$$

Therefore, the phasors of the primary current and the secondary current are expressed as follows:

$$\dot{I}_1 = \frac{R_2 V_1 + \frac{2\sqrt{2}}{\pi}\omega_0 L_m V_{dc}}{R_1 R_2 + (\omega_0 L_m)^2} \quad (15)$$

$$\dot{I}_2 = j\frac{\omega_0 L_m V_1 - \frac{2\sqrt{2}}{\pi} R_1 V_{dc}}{R_1 R_2 + (\omega_0 L_m)^2}. \quad (16)$$

3.2 Estimation equation of primary voltage

From eq. (16), the average current I_{dc} from the rectifier to the DC-DC converter is expressed as follows:

$$I_{dc} = \frac{2\sqrt{2}}{\pi}\frac{\omega_0 L_m V_1 - \frac{2\sqrt{2}}{\pi} R_1 V_{dc}}{R_1 R_2 + (\omega_0 L_m)^2}. \quad (17)$$

If the mutual inductance does not change drastically, the primary voltage is obtained by the estimation equation, which is described as follows:

$$\hat{V}_1 = \frac{\frac{2\sqrt{2}}{\pi} R_1 V_{dc} + \frac{\pi}{2\sqrt{2}}\left\{R_1 R_2 + (\omega_0 L_m)^2\right\} I_{dc}}{\omega_0 L_m}. \quad (18)$$

Then, the DC voltage V_{dc} is already obtained for the secondary voltage control. As a result, the current sensor is only needed as an additional sensor to measure the inflowing current I_{dc}.

4 Power Control on Vehicle side

4.1 Control strategy

Power control is implemented by secondary voltage control using the DC-DC converter on the vehicle-side. The block diagram of the power control is shown in Figure 6. In order to apply linear control theory to the secondary voltage control, an equilibrium point of the DC-DC converter has to be defined properly.

Figure 7 shows the block diagram of the equilibrium point calculation. The equilibrium point, which achieves the required power P^*, is defined as V_{dc}^*, I_{dc}, I_L, and D. Firstly, V_{dc}^* has to be determined to satisfy a constraint on the charging power of WPT. In order to obtain V_{dc}^*, the primary voltage has to be estimated and the estimation equation requires the DC voltage v_{dc} and the inflowing current i_{dc}.

By the equilibrium point calculation, the secondary voltage controller can be designed and the required power P^* can be achieved.

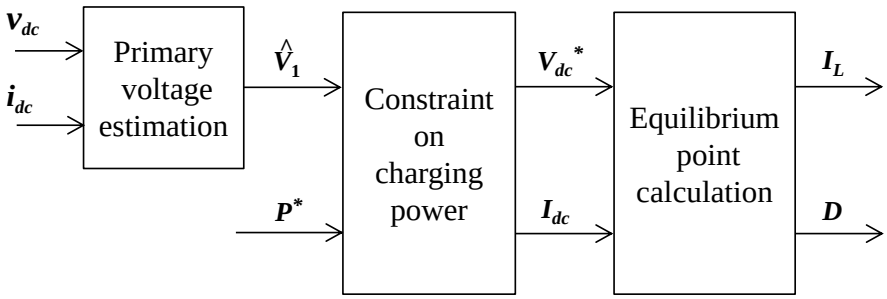

Figure 7: Block diagram of equilibrium point calculation.

4.2 Modeling of DC-DC converter

Figure 8 shows the circuit configuration of the DC-DC converter, where E is battery voltage, L is inductance of the reactor coil, r is internal resistance of the reactor coil and the battery, C is capacitance of the DC-link capacitor, v_{dc} is DC-link voltage, and i_L is the average current flowing into the battery. Assuming that the resonant frequency of WPT is much higher than the switching frequency of the DC-DC converter, i_{dc} is defined as the average current flowing into the DC-link capacitor.

This paper expresses the plant model of the DC-DC converter using the state space averaging method [20]. Then, the DC-DC converter is operated in a continuous conduction mode. When $d(t)$ is defined as the duty cycle of the upper switch, the state space model of the DC-DC converter is indicated as follows:

$$\frac{d}{dt}\boldsymbol{x}(t) = \boldsymbol{A}(d(t))\boldsymbol{x}(t) + \boldsymbol{B}\boldsymbol{u}(t) \qquad (19)$$

$$v_{dc}(t) = \boldsymbol{c}\boldsymbol{x}(t) \qquad (20)$$

$$\boldsymbol{A} := \begin{bmatrix} -\frac{r}{L} & \frac{d(t)}{L} \\ -\frac{d(t)}{C} & 0 \end{bmatrix} \quad \boldsymbol{B} := \begin{bmatrix} -\frac{1}{L} & 0 \\ 0 & \frac{1}{C} \end{bmatrix}$$

$$\boldsymbol{c} := \begin{bmatrix} 0 & 1 \end{bmatrix}$$

$$\boldsymbol{x}(t) := \begin{bmatrix} i_L(t) \\ v_{dc}(t) \end{bmatrix} \quad \boldsymbol{u}(t) := \begin{bmatrix} E \\ i_{dc}(t) \end{bmatrix}.$$

This plant model shows that the DC-DC converter is a non-linear system. In order to use linear control theory, we linearize the state space model around the equilibrium point, which is given as I_L, V_{dc}, I_{dc}, and D. The linearized model is expressed as follows:

$$\frac{d}{dt}\Delta\boldsymbol{x}(t) = \Delta\boldsymbol{A}\Delta\boldsymbol{x}(t) + \Delta\boldsymbol{B}\Delta\boldsymbol{u}(t) \qquad (21)$$

$$\Delta v_{dc}(t) = \Delta\boldsymbol{c}\Delta\boldsymbol{x}(t) \qquad (22)$$

$$\Delta\boldsymbol{A} := \begin{bmatrix} -\frac{r}{L} & \frac{D}{L} \\ -\frac{D}{C} & 0 \end{bmatrix} \quad \Delta\boldsymbol{B} := \begin{bmatrix} \frac{V_{dc}}{L} & 0 \\ -\frac{I_L}{C} & \frac{1}{C} \end{bmatrix}$$

$$\Delta\boldsymbol{c} := \begin{bmatrix} 0 & 1 \end{bmatrix}$$

$$\boldsymbol{x}(t) := \boldsymbol{X} + \Delta\boldsymbol{x}(t)$$

$$\boldsymbol{X} := \begin{bmatrix} I_L \\ V_{dc} \end{bmatrix} \quad \Delta\boldsymbol{x}(t) := \begin{bmatrix} \Delta i_L(t) \\ \Delta v_{dc}(t) \end{bmatrix}$$

$$\boldsymbol{u}(t) := \boldsymbol{U} + \Delta\boldsymbol{u}(t)$$

$$\boldsymbol{U} := \begin{bmatrix} D \\ I_{dc} \end{bmatrix} \quad \Delta\boldsymbol{u}(t) := \begin{bmatrix} \Delta d(t) \\ \Delta i_{dc}(t) \end{bmatrix}.$$

The equilibrium point has to satisfy constraint equations, which are indicated as follows:

$$I_L = \frac{I_{dc}}{D} \qquad (23)$$

$$V_{dc} = \frac{ED - rI_{dc}}{D^2}. \qquad (24)$$

By the linearization of eq. (17), Δi_{dc} is also expressed as follows:

$$\Delta i_{dc} = -\frac{8}{\pi^2}\frac{R_1}{R_1R_2 + (\omega_0 L_m)^2}\Delta v_{dc}. \qquad (25)$$

Therefore, the linearized plant model can be transformed as follows:

$$\frac{d}{dt}\boldsymbol{x}(t) = \boldsymbol{A}\big(d(t)\big)\boldsymbol{x}(t) + \boldsymbol{B}\boldsymbol{u}(t) \tag{26}$$

$$v_{dc}(t) = \boldsymbol{c}\boldsymbol{x}(t) \tag{27}$$

$$\Delta\boldsymbol{A} := \begin{bmatrix} -\frac{r}{L} & \frac{D}{L} \\ -\frac{D}{C} & -\frac{8}{\pi^2}\frac{R_1}{C\left\{R_1R_2 + (\omega_0 L_m)^2\right\}} \end{bmatrix}$$

$$\Delta\boldsymbol{B} := \begin{bmatrix} \frac{V_{dc}}{L} \\ -\frac{I_L}{C} \end{bmatrix} \quad \Delta\boldsymbol{c} := \begin{bmatrix} 0 & 1 \end{bmatrix}$$

$$\boldsymbol{x}(t) := \boldsymbol{X} + \Delta\boldsymbol{x}(t)$$

$$\boldsymbol{X} := \begin{bmatrix} I_L \\ V_{dc} \end{bmatrix} \quad \Delta\boldsymbol{x}(t) := \begin{bmatrix} \Delta i_L(t) \\ \Delta v_{dc}(t) \end{bmatrix}$$

$$\boldsymbol{u}(t) := \boldsymbol{U} + \Delta\boldsymbol{u}(t)$$

$$\boldsymbol{U} := D \quad \Delta\boldsymbol{u}(t) := \Delta d(t).$$

From this model, the transfer function from $\Delta d(s)$ to Δv_{dc} is given as follows:

$$\Delta P_v(s) = \frac{\Delta v_{dc}}{\Delta d} = \frac{b_1 s + b_0}{s^2 + a_1 s + a_0} \tag{28}$$

$$a_1 := \frac{r}{L} + \frac{8}{\pi^2}\frac{R_1}{C\left\{R_1R_2 + (\omega_0 L_m)^2\right\}}$$

$$a_0 := \frac{1}{LC}\left\{D^2 + \frac{8}{\pi^2}\frac{rR_1}{R_1R_2 + (\omega_0 L_m)^2}\right\}$$

$$b_1 := \frac{I_L}{C} \quad b_0 = \frac{rI_L - DV_{dc}}{LC}.$$

4.3 Definition of the equilibrium point

The equilibrium point is defined to achieve the required power P^*. $V_{dc}{}^*$ is calculated by a reference value of the secondary voltage V_2^*, which is obtained by eq. (11), and a Fourier series expansion. Then the primary voltage is obtained by the estimation equation, which is expressed as eq. (18). I_{dc} is determined by the parameters of the WPT circuit and obtained by eq. (17). I_L, and D is given by eq. (23) and (24).

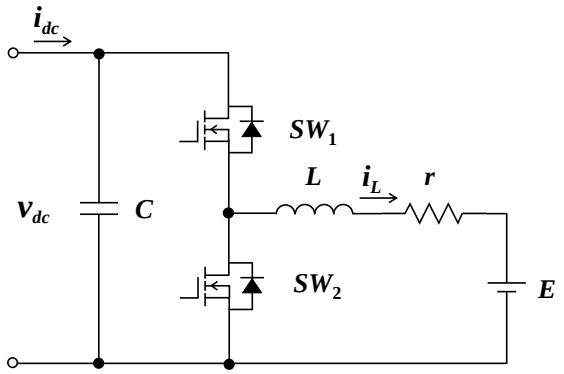

Figure 8: Circuit configuration of DC–DC converter.

Therefore, the equilibrium point can be defined as follows:

$$V_{dc}{}^* = \frac{\pi}{2\sqrt{2}} V_2^*\left(\hat{V}_1, P^*\right) \tag{29}$$

$$I_{dc} = \frac{2\sqrt{2}}{\pi}\frac{\omega_0 L_m \hat{V}_1 - \frac{2\sqrt{2}}{\pi} R_1 V_{dc}{}^*}{R_1R_2 + (\omega_0 L_m)^2} \tag{30}$$

$$D = \frac{E + \sqrt{E^2 - 4rV_{dc}{}^* I_{dc}}}{2V_{dc}} \tag{31}$$

$$I_L = \frac{I_{dc}}{D}. \tag{32}$$

By substituting from eq. (29) to eq. (32) into eq. (28), the transfer function $\Delta P_v(s)$ can be calculated. As a result, the feedback controller for the secondary voltage control can be designed using linear control theory. If a PID controller is applied as the feedback controller, we can design the PID gain using the pole placement method. The PID controller is expressed as follows:

$$C_{PID}(s) = K_P + \frac{K_I}{s} + \frac{K_D s}{\tau_D s + 1}. \tag{33}$$

5 Experiment

5.1 Experimental setup

The wireless power transfer system for power control is shown in Figure 9. In this paper, the motor drive system is neglected, as this is a fundamental study. The experimental equipment is shown in Figure 10. The characteristics of the transmitter and the receiver are indicated in Table 1 and the specification of the DC-DC converter is

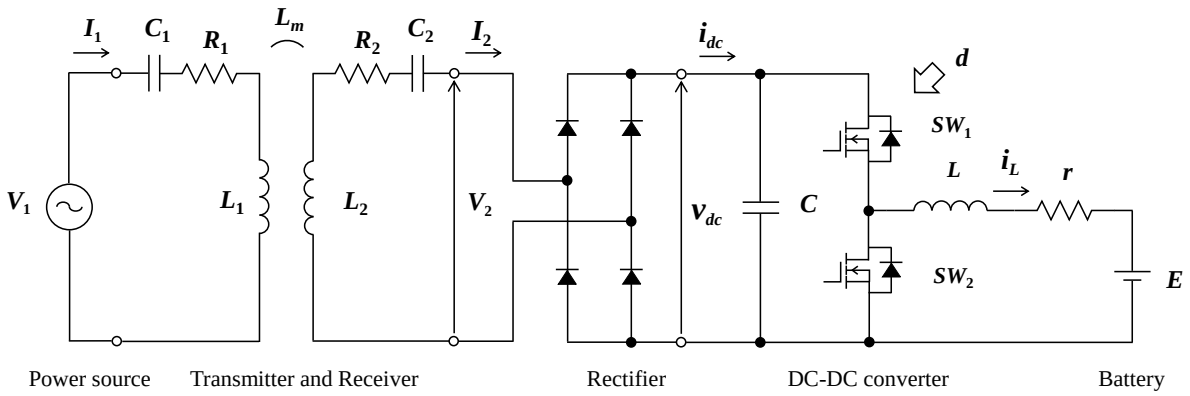

Figure 9: Wireless power transfer system for power control on vehicle-side.

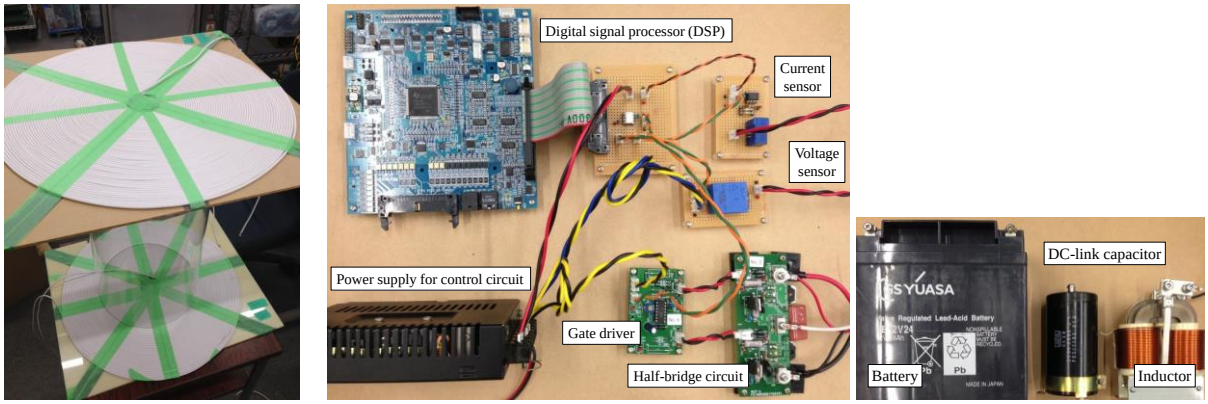

(a) Transmitter and receiver. (b) DC-DC converter.

Figure 10: Experimental equipment.

Table 2: Specification of DC-DC converter.

Battery voltage E	12 V
Internal resistance r	800 mΩ
Inductance L	511 μH
Capacitance C	3300 μF
Carrier frequency f_c	10 kHz

Table 3: Mutual inductance between transmitter and receiver in each transmitting distance.

Transmitting distance g [mm]	Mutual inductance L_m [μH]
100	197.9
200	80.8
300	39.2

expressed in Table 2. The switching frequency of the DC-DC converter was set to 10 kHz, which is much lower than the resonance frequency of the WPT. Therefore, the flowing current into the DC-link capacitor can be used as the average value.

The transmitting distance g was set to 100 mm, 200 mm, and 300 mm. Then, the mutual inductance between the transmitter and the receiver for each transmitting distance were measured by a LCR meter (NF Corporation ZM2371). These values are shown in Table 3.
The power source consisted of a function generator (AFG3021B, Tektronix) and a high-speed bipolar amplifier (HSA4014, NF Corporation) and its frequency was set to 99.8 kHz.

5.2 Primary voltage estimation

In the experiment of the primary voltage estimation, the amplitude of the primary voltage V_1 was tuned to 20 V or 30 V at each condition. The DC-DC converter was replaced with an electronic load (PLZ1004W, KIKUSUI) to simulate the constant voltage on the DC-link. The primary voltage was calculated by the DC voltage V_{dc} and the DC current I_{dc}, which were measured by a power analyzer (PPA5530, Newtons4th Ltd.).

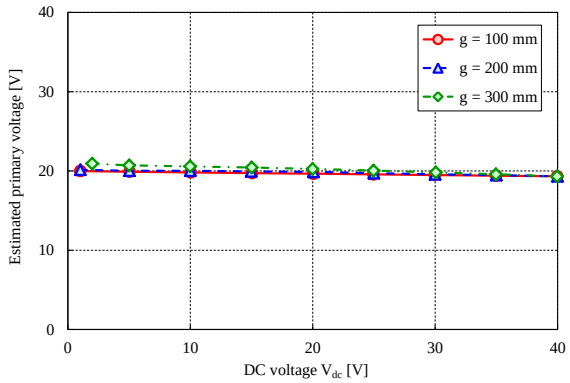

(a) V_1 = 20 V.

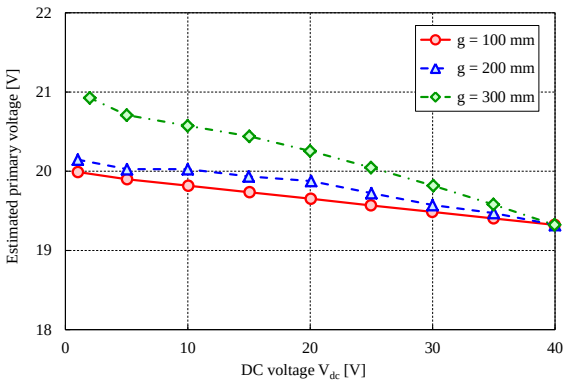

(b) V_1 = 20 V (enlarged view).

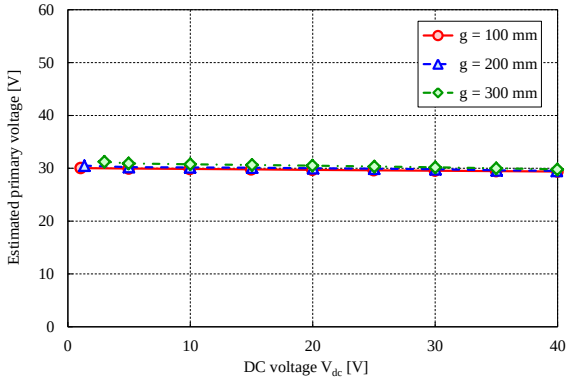

(c) V_1 = 30 V.

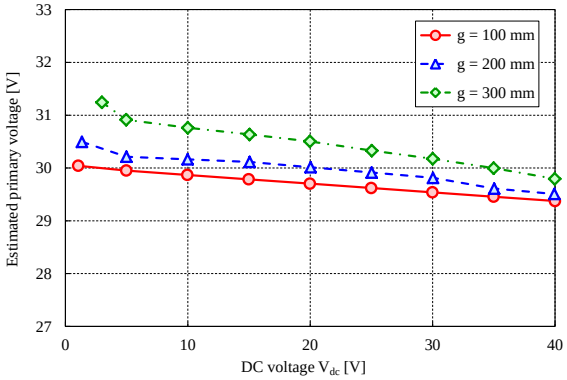

(d) V_1 = 30 V (enlarged view).

Figure 11: Experimental result of primary voltage estimation.

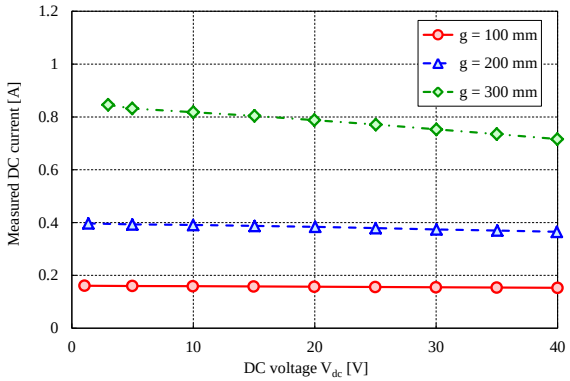

(a) V_1 = 20 V.

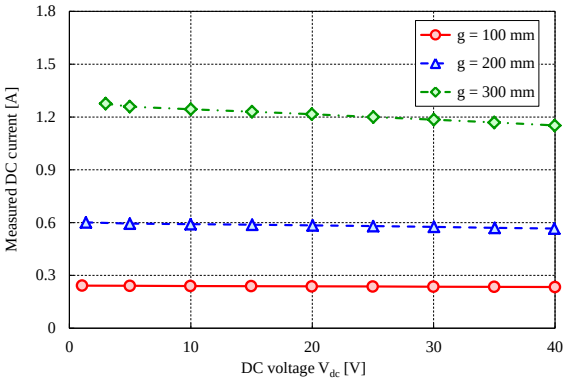

(b) V_1 = 30 V.

Figure 12: Measured DC current at the experiment of primary voltage estimation.

The experimental result is shown in Figure 11. At any transmitting distance, the value calculated by eq. (18) and its true value are closely matched.
The enlarged view indicates a trend, which the estimated primary voltage is decreased as the DC voltage is increased. This trend becomes strong according to the increase in the transmitting distance. Figure 12 indicates that the change in the DC current was increased at long distance transmission. However, the error of the estimated primary voltage, which is shown in Figure 11, is within the allowable range. As a result, the primary voltage estimation can be achieved and used for power control for wireless charging.

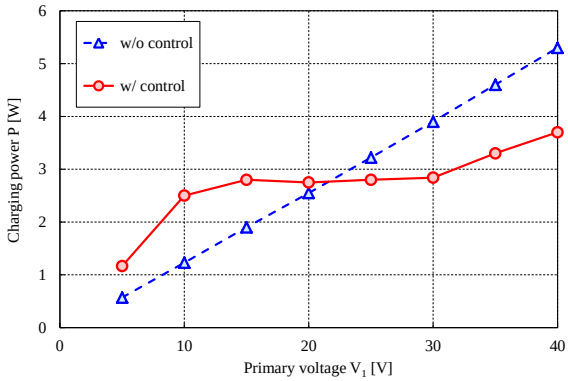

(a) P^* = 2.5 W at 100 mm transmission.

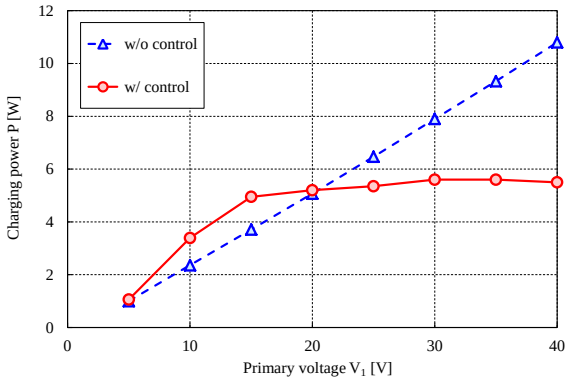

(b) P^* = 5 W at 100 mm transmission.

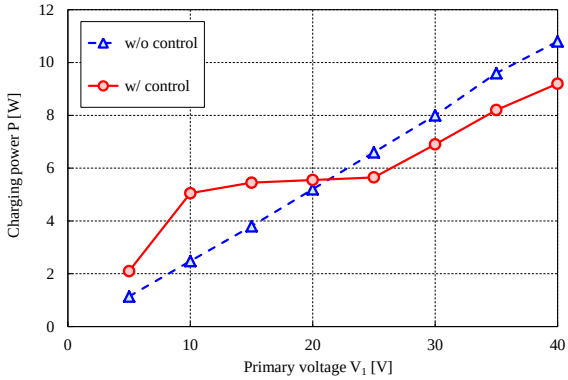

(c) P^* = 5 W at 200 mm transmission.

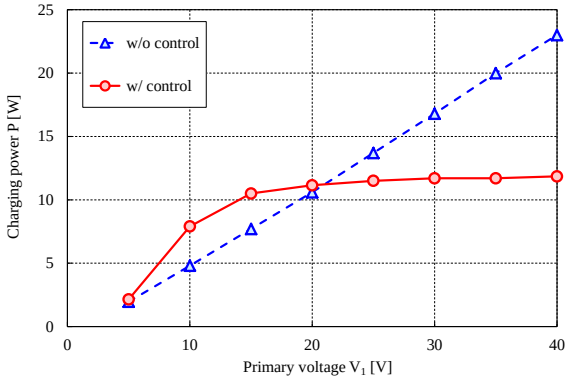

(d) P^* = 10 W at 200 mm transmission.

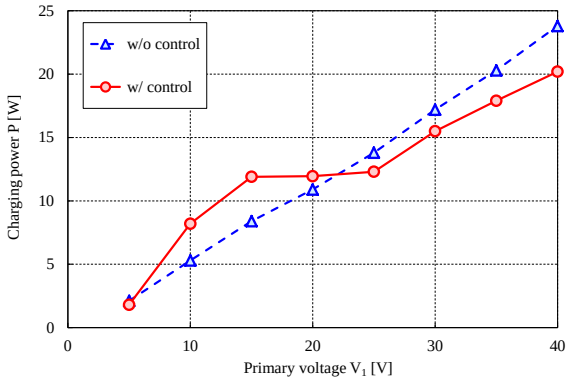

(e) P^* = 10 W at 300 mm transmission.

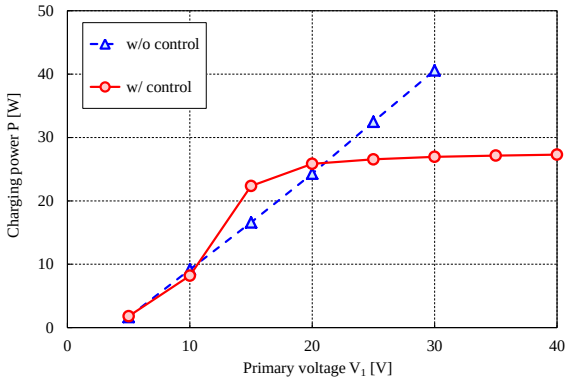

(f) P^* = 20 W at 300 mm transmission.

Figure 13: Experimental result of power control.

5.3 Power control

In order to verify power control based on the primary voltage estimation, secondary voltage control with the equilibrium point calculation was designed and demonstrated. However, in this paper, the feedback controller was not designed and the DC-DC converter was controlled by only *D*. Therefore, secondary voltage control was designed by only the feedforward controller.

Without the control, the equilibrium point was defined to satisfy the required power P^* when the amplitude of the primary voltage was set to 20 V. The experimental result of the power control is shown in Figure 13. When the amplitude of the primary voltage was equated to the design value, the charging power satisfied P^* regardless of the equilibrium point calculation based on the primary voltage estimation. However, when a change in

the primary voltage was occurred, without the control, P^* was not achieved.
On the other hand, by using the equilibrium point calculation based on the primary voltage, the secondary voltage control achieved P^* at the broader operating range. If P^* is not achieved, this is caused by a constraint on the charging power of the WPT circuit or a limitation of the duty cycle of the DC-DC converter. However, the charging power, which was obtained by the proposed method, was much closer to the required power P^* than without the control.
Therefore, it was verified that the power control based on the primary voltage estimation was effective for the dynamic WPT system, which does not have to regulate road-side voltage.

6 Conclusion

This paper proposed a control method based on the primary voltage estimation using only vehicle-side information to simplify ground facilities on a dynamic WPT system. Experiments verified that the primary voltage estimation was achieved and the power control using the equilibrium point calculation based on the primary voltage estimation is effective for the dynamic WPT system, which can be simplified and not be required to regulate the road-side voltage.
In future works, the feedback controller for secondary voltage control, which achieves power control regardless of road-side voltage, will be implemented to reduce the steady-state error. Furthermore, the transient response characteristics of power control and its stability will be discussed.

References

[1] Y. Hori, "Future vehicle driven by electricity and control-research on four-wheel-motored "UOT electric March II"," *IEEE Transactions on Industrial Electronics*, vol. 51, no. 5, pp. 954-962, Oct. 2004.

[2] M. Yilmaz, V. T. Buyukdegirmenci, and P. T. Krein, "General design requirements and analysis of roadbed inductive power transfer system for dynamic electric vehicle charging," in *Proc.2012 IEEE Transportation Electrification Conference and Expo*, 2012, pp. 1-6.

[3] S. Raabe and G. A. Covic, "Practical design considerations for contactless power transfer quadrature pick-ups," *IEEE Transactions on Industrial Electronics*, vol. 60, no.1, pp.400-409, Jan. 2013.

[4] K. Throngnumchai, A. Hanamura, Y. Naruse, and K. Takeda, "Design and evaluation of a wireless power transfer system with road embedded transmitter coils for dynamic charging of electric vehicles," in *Proc.The 27th International Electric Vehicle Symposium and Exhibition*, 2013, pp. 1-5.

[5] S. Lee, B. Choi, and C. T. Rim, "Dynamics characterization of the inductive power transfer system for online electric vehicles by Laplace phasor transform," *IEEE Transactions on Power Electronics*, vol. 28, no. 12, pp. 5902-5909, Dec. 2013.

[6] J. Shin, S. Shin, Y. Kim, S. Ahn, S. Lee, G. Jung, S. Jeon, and D. Cho, "Design and implementation of shaped magnetic-resonance-based wireless power transfer system for roadway-powered moving electric vehicles," *IEEE Transactions on Industrial Electronics*, vol. 61, no. 3, pp. 1179-1192, Mar. 2014.

[7] G. R. Nagendra, L. Chen, G. A. Covic, and J. T. Boys, "Detection of EVs on IPT highways," *IEEE Journal of Emerging and Selected Topics in Power Electronics*, vol. 2, no. 3, pp. 584-597, Sep. 2014.

[8] K. Lee, Z. Pantic, and S. M. Lukic, "Reflexive field containment in dynamic inductive power transfer systems," *IEEE Transactions on power Electronics*, vol. 29, no. 9, pp. 4592-4602, Sep. 2014.

[9] A. Kurs, A. Karalis, R. Moffatt, J. D. Joannopoulos, P. Fisher, and M. Soljacic, "Wireless power transfer via strongly coupled magnetic resonance," *Science Express on 7 June 2007*, vol. 317, no. 5834, pp. 83-86, Jun. 2007.

[10] T. Imura, T. Uchida, and Y. Hori, "Flexibility of contactless power transfer using magnetic resonance coupling to air gap and misalignment for EV," *World Electric Vehicle Association Journal*, vol. 3, pp. 1-10, 2010.

[11] M. Kato, T. Imura, and Y. Hori, "New characteristics analysis considering transmission distance and load variation in wireless power transfer via magnetic resonant coupling," in *Proc. IEEE 34th International Telecommunications Energy Conference*, 2012, pp. 1-5.

[12] S. Li and C. C. Mi, "Wireless power transfer for electric vehicle applications," *IEEE Journal of Emerging and Selected Topics in Power Electronics*, vol. PP, no. 99, pp. 1-14, Apr. 2014.

[13] Y. Moriwaki, T. Imura, and Y. Hori, "Basic study on reduction of reflected power using DC/DC converters in wireless power transfer system via magnetic resonant coupling," in *Proc. IEEE 33rd International Telecommunications Energy Conference*, 2011, pp. 1-5.

[14] K. Iimura, N. Hoshi, and J. Haruna, "Experimental discussion on inductive type contactless power transfer system with boost or buck converter connected to rectifier," in *Proc. IEEE 7th*

International Power Electronics and Motion Control Conference, 2012, vol. 4, pp. 2652-2657.

[15] K. Takuzaki and N. Hoshi, "Consideration of operating condition of secondary-side converter of inductive power transfer system for obtaining high resonant circuit efficiency," *IEE Japan Transactions on Industry Applications*, vol. 132, no. 10, pp. 966-975, Oct. 2012. (in Japanese)

[16] H. Ishihara, F. Moritsuka, H. Kudo, S. Obayashi, T. Itakura, A. Matsushita, H. Mochikawa, and S. Otaka, "A voltage ratio-based efficiency control method for 3 kW wireless power transmission," in *Proc. The 29th Annual IEEE Applied Power Electronics Conference and Exposition*, 2014, pp. 1312-1316.

[17] M. Kato, T. Imura, and Y. Hori, "Study on maximize efficiency by secondary side control using DC-DC converter in wireless power transfer via magnetic resonant coupling," in *Proc. The 27th International Electric Vehicle Symposium and Exhibition*, 2013, pp. 1-5.

[18] T. Imura and Y. Hori, "Maximizing air gap and efficiency of magnetic resonant coupling for wireless power transfer using equivalent circuit and Neumann formula," *IEEE Transactions on Industrial Electronics*, vol. 58, no. 10, pp. 4746-4752, Oct. 2011.

[19] D. Gunji, T. Imura, and H. Fujimoto, "Fundamental research of power conversion circuit control for wireless in-wheel motor using magnetic resonance coupling," in *Proc. 40th Annual Conference of the IEEE Industrial Electronics Society*, 2014, pp. 3004-3009.

[20] D. Takei, H. Fujimoto, and Y. Hori, "Load current feedforward control of boost converter for downsizing output filter capacitor," in *Proc. 40th Annual Conference of the IEEE Industrial Electronics Society*, 2014, pp. 1581-1586.

Authors

Mr. Katsuhiro Hata received his B.E. in electrical engineering from Ibaraki National College of Technology, Ibaraki, Japan, in 2013. He is currently working toward a M.S. degree at the Graduate School of Frontier Sciences with the University of Tokyo. His research interests are mainly on wireless power transfer via magnetic resonant couplings.

Dr. Takehiro Imura received his B.S. in electrical and electronics engineering from Sophia University, Tokyo, Japan. He received his M.S degree and Ph.D. in Electronic Engineering from The University of Tokyo in March 2007 and March 2010 respectively. He is currently a research associate in the Graduate School of Frontier Sciences in the same university.

Dr. Yoichi Hori received his Ph.D. in electrical engineering from The University of Tokyo, Japan, 1983, where he became a Professor in 2000. In 2008, he moved to the Department of Advanced Energy, Graduate School of Frontier Sciences. Prof. Hori was the recipient of the Best Paper Award from the IEEE Transactions on Industrial Electronics in 1993, 2001 and 2013 and of the 2000 Best Paper Award from the Institute of Electrical Engineers of Japan (IEEJ). He is the Chairman of the Motor Technology Symposium of the Japan Management Association.